Order-Recursive Gaussian Elimination (ORGE) and Efficient CAD of Microwave Circuits

Pradeep Misra, *Member, IEEE,* and Krishna Naishadham, *Member, IEEE*

Abstract— **Planar circuit elements in millimeter-wave integrated circuits (MMIC's) typically consist of one or more discontinuities (e.g., stubs) connected to a number of transmission lines. In the computer-aided design (CAD) and optimization of such passive elements using the method of moments, it is necessary to iteratively simulate many subproblems involving dimensional changes to various parts of the circuit. On examining the simulation problem closely, it can be seen that there is a considerable overlap of data in various subproblems. In practice, each subproblem is solved independent of others, without taking into account the duplication of data. This leads to an inefficient design technique. In this paper, we present a design technique that effectively exploits the duplication of data by employing a recursive variant of Gaussian elimination, called order-recursive Gaussian elimination (ORGE). The potential utility of ORGE in microwave circuit simulation and CAD is demonstrated by applying it to the design of a microstrip filter.**

I. Introduction

THE METHOD of moments (MoM) is widely used in the simulation and computer-aided design (CAD) of microwave and millimeter-wave integrated circuits (MMIC's) [1]–[12]. In the MoM, the boundary value problem for the unknown current distribution over the surface of the conductors is formulated as an electrical field integral equation (EFIE). The EFIE is then converted into a system of linear algebraic equations (for the current) by the application of suitable basis and testing functions. The circuit characteristics, such as S-parameters, radiation, and metallization losses, etc., can be derived from the computed current distribution. The current distribution can be solved by implementing the MoM algorithm either in the space domain [1] or in the spectral domain [4].

The system (or moment) matrix that represents the electromagnetic (EM) interactions between basis and test elements used to solve for the current distribution is typically dense. For moderately high-order models ($\mathcal{O}(100 - 500)$), the current distribution may be obtained by resolving the system of linear algebraic equations using LU decomposition and subsequent solution of two triangular systems of equations. The computational complexity of the solution of system of equations of order N is N^3. For several applications in MMIC simulation where N is fixed and moderately small, use of conventional method (via LU decomposition) of solution of system of moment equations is adequate.

Manuscript received July 31, 1995; revised August 26, 1996.

The authors are with the Department of Electrical Engineering, Wright State University, Dayton, OH 45435 USA.

Publisher Item Identifier S 0018-9480(96)08483-9.

In certain situations, however, the order of systems of equations to be solved may change from N to $N + M$, where the original $(N \times N)$ moment matrix becomes a submatrix of the higher-order $(N+M)\times(N+M)$ matrix as a result of augmenting the model. The order M of augmentation is usually not known *a priori* in iterative design tasks. This is frequently encountered in characterization of MMIC elements where the moment matrix is recursively augmented with new row and column vectors that correspond, for example, to circuit extensions, stubs, etc., required to tune a filter or to impedance-match an amplifier. At present, each augmented matrix is treated as a new data matrix and the solution of the augmented system of equations is recomputed from scratch. The resulting solution procedure becomes computationally inefficient, and, as shown later, in the worst case, the computational complexity can become $\mathcal{O}((N + M)^4)$. The primary objective of this paper is to apply a variant of Gaussian elimination, called order-recursive Gaussian elimination (ORGE) [13], to develop a solution procedure of computational complexity $\mathcal{O}((N + M)^3)$. This order of magnitude reduction in computations is clearly very attractive for the CAD of MMIC's.

There are also situations encountered in MMIC design where one iteratively decreases the size or spacing of certain elements in a circuit to meet the design specifications. Consider, for example, the reduction in stub length or stub spacing in the optimization of a low-pass filter, or the reduction in width of a section of microstrip quarter-wave transformer to compensate for dispersion. In these situations, the moment matrix is affected by removal of (or, is decremented by) certain row or column vectors associated with the changes in the circuit. As in augmented systems, the order of decrementation is not known *a priori*. At present, the solution of each decremented system of equations is recomputed from scratch. We introduce an order-recursive Gaussian elimination procedure to solve decremented systems as well, wherein the solution (specifically, the Gaussian elimination) from the prior iteration is used to efficiently solve the reduced system of equations at the present iteration.

In the next section, we present two examples pertaining to MMIC simulation, namely, discontinuity characterization, and interactive filter design and demonstrate how augmented matrices can be constructed in typical problems so as to exploit the computational advantages of ORGE. The same considerations of augmented matrices apply to decremented matrices as well; hence, the construction of decremented systems in the context of MMIC simulation is not discussed. In Section III, the ORGE algorithms for the solution of augmented

and decremented systems are introduced and validated by application to the MoM solution of the current distribution over a rectangular strip in free space. The intent in solving such a simple example is to show how a typical planar problem involving orthogonal currents may be cast in the ORGE framework and to demonstrate the accuracy of the ORGE-computed currents in comparison with a reference solution [14]. The computational complexity of the ORGE algorithm is also discussed in Section III. In Section IV, we apply the augmented ORGE algorithm to the interactive design of a microstrip band-stop (or notch) filter [12] and establish corroboration with measured data. The filter is realized by connecting two stubs on either side of a transmission line. Either the spacing between the stubs or their length is successively increased at each iteration. This simulation exemplifies the enhancement in computational efficiency permitted by the ORGE algorithm for augmented systems. It is straightforward to apply the decremented ORGE in situations where the stub length or spacing has to be decreased during a design iteration. Both augmented and decremented order-recursive techniques have been applied to resolve large moment systems in iterative design problems using LU decomposition [15]. These two contributions, namely ORGE and ORLUD, have been combined into a general framework of MoM implementation, called order-recursive method of moments (ORMoM), which facilitates EM simulation-based microwave CAD and optimization with significant computational advantage over existing linear system solvers [16]. The concluding remarks are summarized in Section V.

II. Augmented Matrix Model of MMIC

A. Discontinuity Analysis

As an example of MMIC analysis where augmented matrices discussed earlier occur, consider the two-port microstrip discontinuity shown in Fig. 1(a). The input and output ports are connected by transmission lines at reference planes 1 and 2 to shunt terminations (at 1′ and 2′). Application of MoM to this circuit yields total currents on the whole structure, including the connection lines. It is necessary to calculate complex amplitudes of the incident and reflected currents at planes 1 and 2 by discarding the influence of port connection lines and the excitation—a process known as de-embedding. Note that the discontinuity in Fig. 1(a) is excited by a shunt current source impressed at the input port by a coaxial cable. De-embedding requires the solution of additional subproblems such as the cascade of the input and output lines [Fig. 1(b)] and a line terminated in a short circuit [Fig. 1(c)] to transform the open-circuit impedance (or Z-parameter) matrix from planes (1′, 2′) to (1, 2) [17]. Alternatively, one could determine the complex amplitude of the incident wave at port 1 from the transmission line model in Fig. 1(b), assuming that the line is long enough to neglect the reflection from the open end at the output port, and embed it in the solution of Fig. 1(a) to compute the S-parameters [18]. The latter approach is used in this paper to arrive at the augmented matrix model of the circuit.

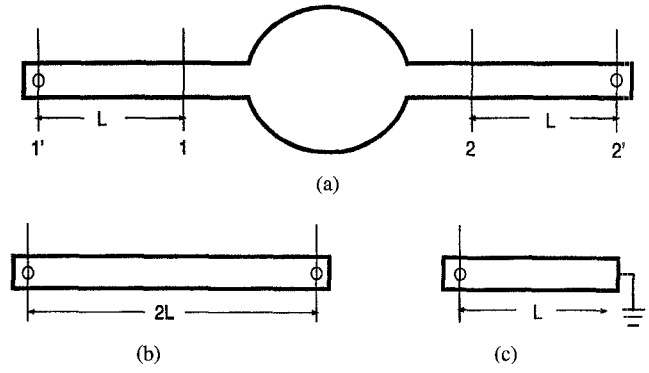

Fig. 1. (a) A two-port microstrip discontinuity. (b) De-embedding line cascaded to its mirror image. (c) De-embedding line terminated in a short circuit.

Some authors have employed spectral estimation techniques such as generalized pencil of functions [2], [19] and Prony's method [20] to directly decompose the total port currents into incident and reflected components. In the absence of computational "noise" of any significance, however, it appears that the computational advantage of these methods, namely, lack of the need to solve auxiliary problems for deembedding the circuit parameters, is offset by the added complexity of the estimation algorithms.

Assume that the input and output lines (of length L) support N_i and N_o basis elements, and the discontinuity (between planes 1 and 2) supports N_d basis elements. Then, the matrix equations resulting from application of MoM to the circuit elements in Fig. 1(a) and 1(b), respectively, can be written as

$$\begin{bmatrix} \boldsymbol{Z}^{ii} & \boldsymbol{Z}^{id} & \boldsymbol{Z}^{io} \\ \boldsymbol{Z}^{di} & \boldsymbol{Z}^{dd} & \boldsymbol{Z}^{do} \\ \boldsymbol{Z}^{oi} & \boldsymbol{Z}^{od} & \boldsymbol{Z}^{oo} \end{bmatrix} \begin{bmatrix} \boldsymbol{I}^{i} \\ \boldsymbol{I}^{d} \\ \boldsymbol{I}^{o} \end{bmatrix} = \begin{bmatrix} \boldsymbol{V}^{i}_{\text{inc}} \\ \boldsymbol{V}^{d}_{\text{inc}} \\ \boldsymbol{V}^{o}_{\text{inc}} \end{bmatrix} \tag{1}$$

$$\begin{bmatrix} \boldsymbol{Z}^{ii} & \boldsymbol{Z}^{io} \\ \boldsymbol{Z}^{oi} & \boldsymbol{Z}^{oo} \end{bmatrix} \begin{bmatrix} \boldsymbol{I}^{iL} \\ \boldsymbol{I}^{oL} \end{bmatrix} = \begin{bmatrix} \boldsymbol{V}^{i}_{\text{inc}} \\ \boldsymbol{V}^{o}_{\text{inc}} \end{bmatrix}. \tag{2}$$

Knowing the port currents from the solution of (1) and (2), the two independent S-parameters for a symmetrical two-port may be computed as

$$S_{11} = -\frac{I_1^i - I_1^{iL}}{I_1^{iL}}, \quad S_{21} = \frac{I_2^o}{I_1^{iL}}. \tag{3}$$

It is evident from (1) and (2) that the system matrix in (2) is a submatrix of the matrix in (1). Therefore, if (2) is solved first, it should be possible to embed its solution in (1) to make the solution of (1) more efficient. Note that the block sub-matrices of the system matrix in (1) may be rearranged to obtain

$$\left[\begin{array}{cc|c} \boldsymbol{Z}^{ii} & \boldsymbol{Z}^{io} & \boldsymbol{Z}^{id} \\ \boldsymbol{Z}^{oi} & \boldsymbol{Z}^{oo} & \boldsymbol{Z}^{od} \\ \hline \boldsymbol{Z}^{di} & \boldsymbol{Z}^{do} & \boldsymbol{Z}^{dd} \end{array}\right] \left[\begin{array}{c} \boldsymbol{I}^{i} \\ \boldsymbol{I}^{o} \\ \hline \boldsymbol{I}^{d} \end{array}\right] = \left[\begin{array}{c} \boldsymbol{V}^{i}_{\text{inc}} \\ \boldsymbol{V}^{o}_{\text{inc}} \\ \hline \boldsymbol{V}^{d}_{\text{inc}} \end{array}\right]. \tag{4}$$

Clearly, the system (4) is a bordered matrix, obtained by augmenting the system matrix of (2) with the interactions pertinent to the discontinuity, and is referred to as *augmented* matrix model of the discontinuity. In the sequel, it will be discussed how the augmented matrix equation can be solved efficiently.

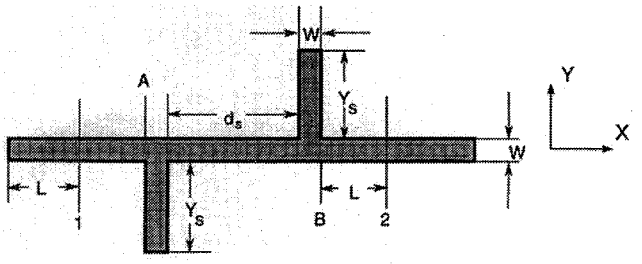

Fig. 2. Microstrip double-stub filter.

B. Interactive Filter Design

The use of ORGE will provide further efficiency in MMIC design applications. Consider the microstrip double-stub filter shown in Fig. 2. The input and output lines indicated by ports 1 and 2 are oriented longitudinally. It is desired to design two stubs (each of length Y_S) such that the filter has a pre-specified cut-off frequency and pass-band roll-off. Once the optimal stub length is determined, the spacing between the stubs, d_s, needs to be tuned to optimize the filter performance. Although the desired filter can be realized using circuit simulation [21], we have considered this example to illustrate the computational advantages of ORGE in microwave CAD.

Assume that the input and output transmission lines (comprised by the x-oriented line excluding the section AB) are gridded such that they support N_i and N_o basis elements, respectively. On applying the MoM, the cascade of these two lines generates a moment matrix, which we will refer to as *line matrix*. The line matrix and the corresponding system of equations for computing line currents are identical to (2). The section AB supports N_{d_0} basis functions, thus generating a self-matrix $\boldsymbol{Z}^{d_0 d_0}$ of order N_{d_0}. The currents along the x-directed line would then contribute the upper left system of sub-matrices shown in (5) at the bottom of the page. Next, suppose that we add two stubs symmetrically on either side of the line (see Fig. 2) and iteratively increase their length (keeping d_s fixed) until the filter response or insertion loss displays the specified cut-off frequency and the pass-band roll-off. During each iteration, an increasingly large-order linear system of equations needs to be solved to verify whether or not the desired response has been achieved. Assume that the stub length is increased successively in M steps, where each iteration contributes additional N_d rows and columns to the system matrix. Then, at the r-th iteration, the system matrix will be of $(N_i + N_o + N_{d_0} + rN_d)$-th order, $r = 1, \cdots, M$. When the interaction of stubs with the line is accounted for, the resulting system matrix at the Mth iteration will have the structure shown in (5), with appropriate voltage vector and the unknown current distribution vector. Therefore, at each iteration, the upper-left system in (5) is augmented by the reaction terms associated with the two stubs. If the stub length is fixed and the stub separation is varied instead, then, the entries corresponding to the stubs may be interchanged with those of the section AB to construct the augmented matrix model of the filter.

III. Order-Recursive Gaussian Elimination

In this section, an order-recursive variant of conventional Gaussian elimination method for computation of $\boldsymbol{x}_r$ in

$$\boldsymbol{A}_r \boldsymbol{x}_r = \boldsymbol{b}_r$$

is presented. The proposed algorithm is developed for the case when *all* the leading principal sub-matrices of the matrix $\boldsymbol{A}$ (whose size is not known *a priori*) are nonsingular. Therefore, the solution (albeit suboptimal) can always be computed without the need of pivoting.

A. The ORGE Algorithm for Augmented Systems

Assume that the Gaussian elimination on $(\boldsymbol{A}_r, \boldsymbol{b}_r)$ has been computed and that for $(\boldsymbol{A}_{r+1}, \boldsymbol{b}_{r+1})$ is desired. On augmenting $\boldsymbol{A}_r$ by an additional row and column and $\boldsymbol{b}_r$ by an additional row, we have the equation shown at the bottom of the next page, where $\eta_{i,j}$ represent the elementary transformation required to eliminate the corresponding element of the original system matrix, $\boldsymbol{a}_{*,r+1}$ denotes the $(r+1)$th column vector, and $\boldsymbol{a}_{r+1,*}$ denotes the $(r+1)$th row vector.

The operations of order-recursive Gaussian elimination can be divided into two major categories.

1) The first category consists of updating the new column of the augmented matrix $\boldsymbol{A}_{r+1}$ such that the effect of row operations performed on the matrix $\boldsymbol{A}_r$ is reflected in the $(r+1)$th column of $\boldsymbol{A}_{r+1}$.
2) The second category consists of the elimination of the elements of $(r+1)$th row to transform the augmented pair $[\boldsymbol{A}_{r+1}, \boldsymbol{b}_{r+1}]$ to an upper trapezoidal form.

Note that due to the assumption of nonsingularity of the leading principal sub-matrices, the above operations are well defined. A detailed explanation of performing the various steps may be found in [22]. For sake of conciseness, we outline

$$\left[\begin{array}{ccc|ccccc} \boldsymbol{Z}^{ii} & \boldsymbol{Z}^{io} & \boldsymbol{Z}^{id_0} & \boldsymbol{Z}^{id_1} & \cdots & \boldsymbol{Z}^{id_r} & \cdots & \boldsymbol{Z}^{id_M} \\ \boldsymbol{Z}^{oi} & \boldsymbol{Z}^{oo} & \boldsymbol{Z}^{od_0} & \boldsymbol{Z}^{od_1} & \cdots & \boldsymbol{Z}^{od_r} & \cdots & \boldsymbol{Z}^{od_M} \\ \boldsymbol{Z}^{d_0 i} & \boldsymbol{Z}^{d_0 o} & \boldsymbol{Z}^{d_0 d_0} & \boldsymbol{Z}^{d_0 d_1} & \cdots & \boldsymbol{Z}^{d_0 d_r} & \cdots & \boldsymbol{Z}^{d_0 d_M} \\ \hline \boldsymbol{Z}^{d_1 i} & \boldsymbol{Z}^{d_1 o} & \boldsymbol{Z}^{d_1 d_0} & \boldsymbol{Z}^{d_1 d_1} & \cdots & \boldsymbol{Z}^{d_1 d_r} & \cdots & \boldsymbol{Z}^{d_1 d_M} \\ \vdots & \vdots & \vdots & \vdots & \ddots & \vdots & \ddots & \vdots \\ \boldsymbol{Z}^{d_r i} & \boldsymbol{Z}^{d_r o} & \boldsymbol{Z}^{d_r d_0} & \boldsymbol{Z}^{d_r d_1} & \cdots & \boldsymbol{Z}^{d_r d_r} & \cdots & \boldsymbol{Z}^{d_r d_M} \\ \vdots & \vdots & \vdots & \vdots & \ddots & \vdots & \ddots & \vdots \\ \boldsymbol{Z}^{d_M i} & \boldsymbol{Z}^{d_M o} & \boldsymbol{Z}^{d_M d_0} & \boldsymbol{Z}^{d_M d_1} & \cdots & \boldsymbol{Z}^{d_M d_r} & \cdots & \boldsymbol{Z}^{d_M d_M} \end{array}\right] \tag{5}$$

the following algorithm to implement the operations discussed above.

Algorithm A-ORGE: *Augmented Order Recursive Gaussian Elimination*

for $m = 1, \cdots, n-1$

$\boldsymbol{A}_{r+1} = \begin{bmatrix} \boldsymbol{A}_r & \boldsymbol{a}_{*,r+1} \\ \boldsymbol{a}_{r+1,*} & a_{r+1,r+1} \end{bmatrix}; \boldsymbol{b}_{r+1} = \begin{bmatrix} \boldsymbol{b}_r \\ b_{r+1} \end{bmatrix}$

comment: update

for $i = 2, \cdots, r$

$$\begin{bmatrix} a_{i,r+1} \\ \vdots \\ a_{r,r+1} \end{bmatrix} := \begin{bmatrix} a_{i,r+1} \\ \vdots \\ a_{r,r+1} \end{bmatrix} - a_{i-1,r+1} \begin{bmatrix} \eta_{i,i-1} \\ \vdots \\ \eta_{r,i-1} \end{bmatrix}$$

end

comment: triangularize $\boldsymbol{A}_{r+1}$ and update $\boldsymbol{b}_{r+1}$

for $j = 1, \cdots, r$

$\eta_{r+1,j} = a_{r+1,j}/a_{j,j}$

$b_{r+1} := b_{r+1} - \eta_{r+1,j} b_j$

for $k = j+1, \cdots, r$

$a_{r+1,k} := a_{r+1,k} - \eta_{r+1,j} a_{j,k}$

end

$a_{r+1,j} := \eta_{r+1,j}$

end

$r := r+1$

B. The ORGE Algorithm for Decremented Systems

In the previous section, it was shown that knowing the solution of a lower-order system of linear algebraic equations, it is possible to efficiently compute the solution of higher-order systems (obtained by augmentation). Next, the converse problem is addressed: knowing the Gaussian elimination solution of a higher-order system, an efficient procedure for determination of solution for a lower-order system of equations (obtained by deleting some rows and columns of the higher-order system) is developed. Formally, assume that in $\boldsymbol{A}_r \boldsymbol{x}_r = \boldsymbol{b}_r$, the upper triangular elements of $\boldsymbol{A}$ after Gaussian elimination (without pivoting) as well as the pivot entries $\eta_{i,j}$ are known [see (6) at the bottom of the next page].

Then, we wish to compute the solution of $\boldsymbol{A}_\ell \boldsymbol{x}_\ell = \boldsymbol{b}_\ell$, where $\ell < r$.

As in the case of A-ORGE, the operations for the solution of decremented systems of linear algebraic equations may be subdivided into two categories.

1) Updating the rows and columns affected by deletion of ℓth row/column of the system matrix. This causes the numerical values of elements with *both* row and column indexes greater than ℓ to change, thereby, forcing the submatrix in rows and columns $(\ell+1)$ through n change. Then, the following two situations may arise:
   a) $\ell = r-1$: This corresponds to the decremented system where the last row and column of $\boldsymbol{A}_r$ and last row of $\boldsymbol{b}_r$ are deleted. The resulting decremented system consists of the first $(r-1)$ rows and columns of of $\boldsymbol{A}_r$ and first $(r-1)$ rows of $\boldsymbol{b}_r$ (along with the pivot information contained in $\eta_{i,j}$). It is clear that the solution $\boldsymbol{x}_{r-1}$ can be computed by solving the resulting $(r-1)$th order upper triangular system of equations without modifying the parameters of $[\boldsymbol{A}_{r-1} || \boldsymbol{b}_{r-1}]$.
   b) $\ell < r-1$. Here, the ℓth row and column eliminated from $[\boldsymbol{A}_r || \boldsymbol{b}_r]$ affects the elements in $(\ell+1 : r)$ rows and columns of bottom right corner of the matrix $\boldsymbol{A}_r$ and $(\ell+1 : r)$ rows of the vector $\boldsymbol{b}_r$. These elements of matrix $\boldsymbol{A}_r$ and vector $\boldsymbol{b}_r$ must be updated to obtain the correct solution of the system. For additional details, the reader is referred to [22].
2) Gaussian elimination without pivoting of the submatrix in rows and columns $(\ell+1)$ through n.

The algorithm outlined next implements the procedure discussed above.

Algorithm D-ORGE: *Decremented Order Recursive Gaussian Elimination*

comment: update

for $i = r, \cdots, \ell+1$

for $k = i, \cdots, r$

$[a_{k,i-1} \cdots a_{k,r} || b_k] := [a_{k,i-1} \cdots a_{k,r} || b_k] + \eta_{k,i-1} [a_{i-1,i-1} \cdots a_{i-1,r} || b_{i-1}]$

end

end

comment: delete ℓth row and column

Set $[\boldsymbol{A} || \boldsymbol{b}] := \begin{bmatrix} \boldsymbol{A}_{1:\ell-1,1:\ell-1} & \boldsymbol{A}_{1:\ell-1,\ell+1,r} & \| & \boldsymbol{b}_{1\,\ell-1} \\ \boldsymbol{A}_{\ell+1\,r,\ell+1,r} & \boldsymbol{A}_{\ell+1:r,1:\ell-1} & \| & \boldsymbol{b}_{\ell+1\,r} \end{bmatrix}$

comment: triangularize $\boldsymbol{A}_{\ell+1:r,\ell+1:r}$ and update $\boldsymbol{b}_{\ell+1:r}$

for $j = \ell+1, \cdots, r-1$

for $i = j, \cdots, r-1$

$\eta_{i+1,j} = a_{i+1,j}/a_{j,j}$

$[a_{i+1,j} \cdots a_{i+1,r} || b_{i+1}] := [a_{i+1,j} \cdots a_{i+1,r} || b_{i+1}] - \eta_{i+1,j} [a_{j,j} \cdots a_{j,r} || b_j]$

$a_{i+1,j} := \eta_{i+1,j}$

end

end

In the algorithm above, $\boldsymbol{A}_{1:\ell-1,1:\ell-1}$ represents a matrix with row and column indexes $1, \cdots, (\ell-1)$ and $\boldsymbol{b}_{1:\ell-1}$ represents

$$[\boldsymbol{A}_{r+1} || \boldsymbol{b}_{r+1}] := \left[\begin{array}{c|c||c} \boldsymbol{A}_r & \boldsymbol{a}_{*,r+1} & \boldsymbol{b}_r \\ \hline \boldsymbol{a}_{r+1,*} & a_{r+1,r+1} & b_{r+1} \end{array}\right] = \left[\begin{array}{ccc|c||c} a_{11} & a_{12} & \cdots & a_{1,r} & a_{1,r+1} & b_1 \\ \eta_{21} & a_{22} & \cdots & a_{2,r} & a_{2,r+1} & b_2 \\ \vdots & \vdots & \ddots & \vdots & \vdots & \vdots \\ \eta_{r,1} & \eta_{r,2} & \cdots & a_{r,r} & a_{r,r+1} & b_r \\ \hline a_{r+1,1} & a_{r+1,2} & \cdots & a_{r+1,r} & a_{r+1,r+1} & b_{r+1} \end{array}\right]$$

a column vector with row indexes $1, \cdots, (\ell - 1)$. Note that instead of a single row/column, if several rows and columns were to be deleted at the same time, the algorithm D-ORGE can be easily adapted to achieve that. Details have been omitted for the sake of brevity and may be found in [22].

C. Computational Complexity

1) Algorithm A-ORGE: It is clear from the description in Section III-A that the computational complexity of A-ORGE is identical to Gaussian elimination. The only difference is the sequence in which the elimination is performed. Hence, the elimination and back substitution together require $\mathcal{O}(N+M)^3$ operations, where $(N + M)$ is the dimension of the final augmented matrix. However, if a new Gaussian elimination together with back substitution is performed for each system of order $(N + i\hat{M})$, where $i = 0, \cdots, r$ denotes the iteration number, $\hat{M}$ is the number of rows and columns by which the matrix is augmented in each iteration, and $(r\hat{M}) = M$, then the operations count is approximately $\Sigma_{i=0}^{r} (N+i\hat{M})^3$. To see that the latter is an order of magnitude higher than the former, consider the following example.

Let $N = 100, \hat{M} = 10, r = 10$, i.e., we are augmenting the system matrix by ten rows and columns in each iteration and performing a total of ten iterations. The resulting operations count is shown in Fig. 3. Note that since the intent is to observe the order of magnitude complexity, the operations count has been weighted down by $(N + i\hat{M})^3$ for both methods at each iteration. It can be seen clearly that while A-ORGE operations count exhibits a slope of zero (implying $\mathcal{O}(N + M)^3$ operations count), as anticipated, the normalized count for the case when the entire solution is recomputed from scratch shows constant nonzero slope (implying $\mathcal{O}(N+M)^4$). It is evident that the computational savings of A-ORGE are most significant when the iteration count is large.

2) Algorithm D-ORGE: It is evident that the total operations required to update and triangularize the sub-system $[\boldsymbol{A}_{\ell+1:n,\ell+1:n} || \boldsymbol{b}_{\ell+1:n}]$ is twice the cost of Gaussian elimination for a matrix of dimension $(N - \ell)$, where N is the order of the matrix and ℓ is the index of row/column that needs to be eliminated, i.e., $\mathcal{O}(N-\ell)^3$ operations are required for updating and triangularizing operations in Algorithm D-ORGE.

Note that since ℓ cannot be specified *a priori*, it is difficult to give a precise computational count. It suffices to say, however, that intelligent arrangement of the elements of the system matrix would ensure that $(N - \ell) \ll N$. Clearly, performing a completely new Gaussian elimination for each decremented matrix will require approximately $\mathcal{O}(N^3)$ operations, hence the proposed technique can provide significant reduction in the computational cost.

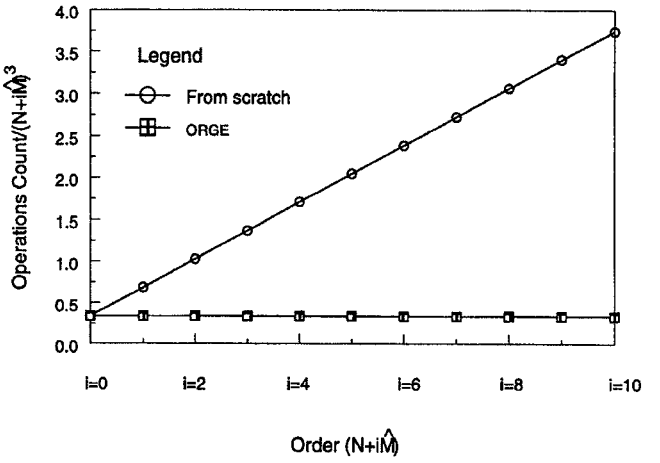

Fig. 3. Order-of-magnitude estimate of operations count.

D. Validation Example

We next consider a simple design problem that serves to validate as well as illustrate the use of ORGE in microwave circuit simulation. We consider the problem of recursively determining the current distribution on a rectangular plate in free space, shown in Fig. 4. The intent of this example is to show how the problem may be cast in the ORGE framework and then to verify that indeed the solution so obtained is accurate. The real impact of ORGE will be seen on considerably higher-order problems. It is also noted that the final plate dimensions are known in this example, hence, we could solve the corresponding system of equations directly instead of recursively building up the solution. Using this simple example, however, we wish also to illustrate that the impedance (or moment) matrix is not necessarily augmented as required by ORGE and how that situation is handled. The construction of the augmented matrix model in this example is directly applicable to circuit geometries of arbitrary shape, where currents in two orthogonal directions need consideration [1].

The plate has dimensions $L = 0.5$ mm and width $W = 0.2$ mm. The current distribution over the plate is computed by the MoM using roof-top basis functions and razor testing [14]. Instead of directly solving for the current over a plate of size 0.5 mm $\times$ 0.2 mm, however, we employ ORGE to recursively

$$\left[\begin{array}{cccc|c|cc||c} a_{11} & a_{12} & \cdots & a_{1,r-3} & a_{1,r-2} & a_{1,r-1} & a_{1,r} & b_1 \\ \eta_{21} & a_{22} & \cdots & a_{2,r-3} & a_{2,r-2} & a_{2,r-1} & a_{2,r} & b_2 \\ \vdots & \vdots & \ddots & \vdots & \vdots & \vdots & \vdots & \vdots \\ \eta_{r-3,1} & \eta_{r-3,2} & \cdots & a_{r-3,r-3} & a_{r-3,r-2} & a_{r-3,r-1} & a_{r-3,r} & b_{r-3} \\ \hline \eta_{r-2,1} & \eta_{r-2,2} & \cdots & \eta_{r-2,r-3} & a_{r-2,r-2} & a_{r-2,r-1} & a_{r-2,r} & b_{r-2} \\ \hline \eta_{r-1,1} & \eta_{r-1,2} & \cdots & \eta_{r-1,r-3} & \eta_{r-1,r-2} & a_{r-1,r-1} & a_{r-1,r} & b_{r-1} \\ \eta_{r,1} & \eta_{r,2} & \cdots & \eta_{r,r-3} & \eta_{r,r-2} & \eta_{r,r-1} & a_{r,r} & b_r \end{array}\right] . \quad (6)$$

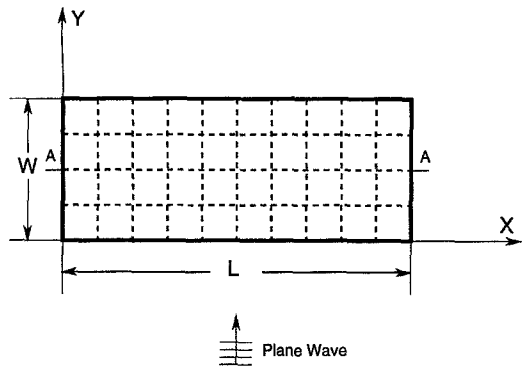

Fig. 4. A rectangular plate in free space.

TABLE I
ORDER OF MATRICES FOR DIFFERENT PLATE DIMENSIONS

M	N	N_x	N_y	Order
4	4	12	12	24
6	4	20	18	38
8	4	28	24	52
10	4	36	30	66

build this solution starting from a 0.2 mm × 0.2 mm plate and uniformly incrementing the plate length in three iterations to 0.5 mm (the width remains unchanged at 0.2 mm). In each iteration, the plate is divided into an appropriate number of square cells, each of side 0.05 mm. Let M and N denote the number of cells along x and y, respectively, while N_x and N_y denote the number of corresponding basis functions. Table I displays the order of the moment matrix, namely, $N_x + N_y$, at each iteration of ORGE.

Because of the orthogonal x- and y-directed currents along the plate surface, the order in which moment matrix elements are filled is not as expected by ORGE. Consider the 4 × 4 (cells) plate which supports 12 basis functions each along the x- and y-directions. The structure of the moment matrix for this plate is given by the matrix

$$Z = \begin{bmatrix} Z_{xx}^{11} & Z_{xy}^{11} \\ Z_{yx}^{11} & Z_{yy}^{11} \end{bmatrix} \tag{7}$$

where each submatrix is of the order 12 × 12. The first and second subscripts indicate testing and expansion current directions. The superscripts indicate that the expansion function and the test path both pertain to the first iteration. When the plate is extended to 6 × 4 cells, each submatrix in (7) is *block-augmented* by the reactions associated with the currents flowing along the plate extension. As shown below, this arrangement will not create a bordered system required by ORGE. With the same notation as in (7), the 6 × 4 plate yields the matrix

$$\left[\begin{array}{cc|cc} Z_{xx}^{11}\ 12\times12 & Z_{xx}^{12}\ 12\times8 & Z_{xy}^{11}\ 12\times12 & Z_{xy}^{12}\ 12\times6 \\ Z_{xx}^{21}\ 8\times12 & Z_{xx}^{22}\ 8\times8 & Z_{xy}^{21}\ 8\times12 & Z_{yy}^{12}\ 8\times6 \\ \hline Z_{yx}^{11}\ 12\times12 & Z_{yx}^{12}\ 12\times8 & Z_{yy}^{11}\ 12\times12 & Z_{yy}^{12}\ 12\times6 \\ Z_{yx}^{21}\ 6\times12 & Z_{yx}^{22}\ 6\times8 & Z_{yy}^{21}\ 6\times12 & Z_{yy}^{22}\ 6\times6 \end{array}\right] \tag{8}$$

where the order of each submatrix is explicitly shown. The second superscript of each submatrix indicates the iteration corresponding to the expansion function, while the first indicates that corresponding to the test path location. For example, with the cells numbered sequentially from iteration to iteration, $Z_{xy^{12}}$ represents the reaction between a y-directed basis element along the plate extension (or second iteration) and a test point along the 4×4 plate considered in the first iteration. The block-augmented system above can be brought to the bordered form [see (4)] by performing appropriate block row and column permutations, yielding the augmented matrix model

$$\left[\begin{array}{cc|cc} Z_{xx}^{11}\ 12\times12 & Z_{xy}^{11}\ 12\times12 & Z_{xx}^{12}\ 12\times8 & Z_{xy}^{12}\ 12\times6 \\ Z_{yx}^{11}\ 12\times12 & Z_{yy}^{11}\ 12\times12 & Z_{yx}^{12}\ 12\times8 & Z_{yy}^{12}\ 12\times6 \\ \hline Z_{xx}^{21}\ 8\times12 & Z_{xy}^{21}\ 8\times12 & Z_{xx}^{22}\ 8\times8 & Z_{xy}^{22}\ 8\times6 \\ Z_{yx}^{21}\ 6\times12 & Z_{yy}^{21}\ 6\times12 & Z_{yx}^{22}\ 6\times8 & Z_{yy}^{22}\ 6\times6 \end{array}\right]. \tag{9}$$

This system is in a form suitable for application of ORGE. The above model can be easily generalized to any iteration. In fact, the same formulation can be applied to the iterative design of any planar structure that supports both x- and y-directed currents.

Fig. 5 displays the real and imaginary parts of the x-directed current along the AA-cut (see Fig. 4) through the center of the plate. The current location is measured by the cell number. As discussed earlier, the plate size is successively extended along the x-direction by two cells at each iteration, starting from a length of four cells. The cell numbers along the x-direction at each iteration are shown in the first column of Table I. Thus, the curve in Fig. 5 for abscissa between zero and four corresponds to the first iteration, that between zero and six corresponds to the second, and so on. The current at each iteration has been computed using ORGE. The complex current in the last iteration has been compared to the direct MoM computation from [14]. It has been found that the two results agree within eight decimal places for both real and imaginary currents. A similar validation has been observed for the y-directed current also, but, it is not presented for brevity. We believe that the accurate calculation of surface current distribution is a much more stringent test of validation than comparisons based on far-field parameters or circuit parameters. All these parameters are ultimately computed using the current distribution determined by the MoM.

IV. Simulation Results

Fig. 6 shows the insertion loss at a few iterations for a microstrip double-stub, notch filter (shown in Fig. 2) on alumina substrate ($\epsilon_r = 9.9, h = 0.127$ mm). The metallization is 5-μm-thick copper ($\sigma_{\text{eff}} = 4.5 \times 10^7$ S/m) and $W = 0.126$ mm. The stub length is increased in five iterations from $Y_S = 1.458$ mm to $Y_S = 2.916$ mm, with the separation fixed at $d_s = 0.756$ mm. The current distribution over the filter is computed at each iteration using an efficient PC-based moment method implementation described in [11], which employs closed-form Green's functions and exploits symmetries and redundancies in the various reactions to fill the moment matrix. The MoM

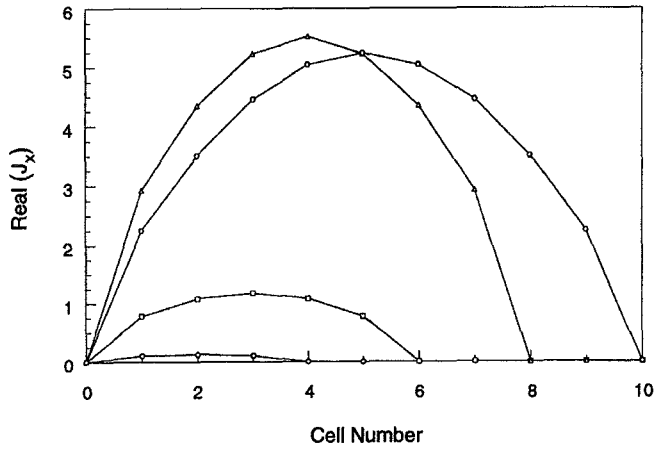

(a)

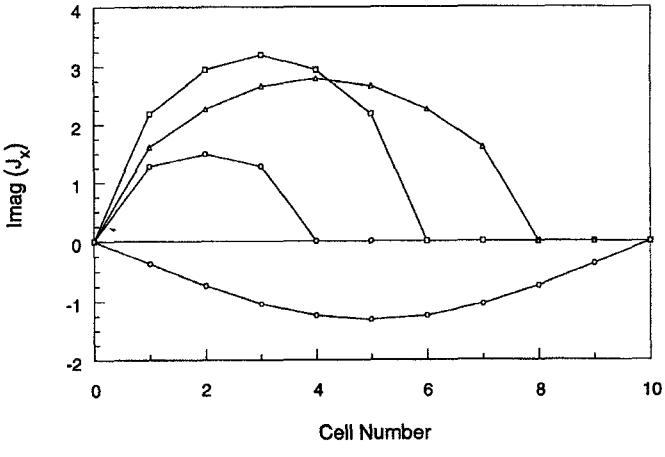

(b)

Fig. 5. Current distribution along AA cut. (a) Real current. (b) Imaginary current.

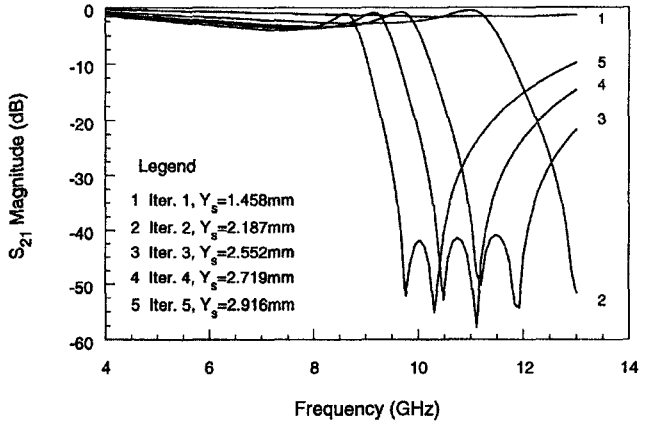

Fig. 6. Iterative double-stub notch filter design: Y_s changing.

algorithm is the mixed potential approach described in [14]. Once filled, the system of linear equations is solved using the ORGE algorithm. The S-parameters are computed at the reference planes located on the input and output lines at a distance of 2 mm from the filtering stub. The de-embedding line segments have length $L = 3$ mm.

Fig. 6 clearly shows that the designed notch frequency of 10 GHz and the notch attenuation of about 40 dB are achieved

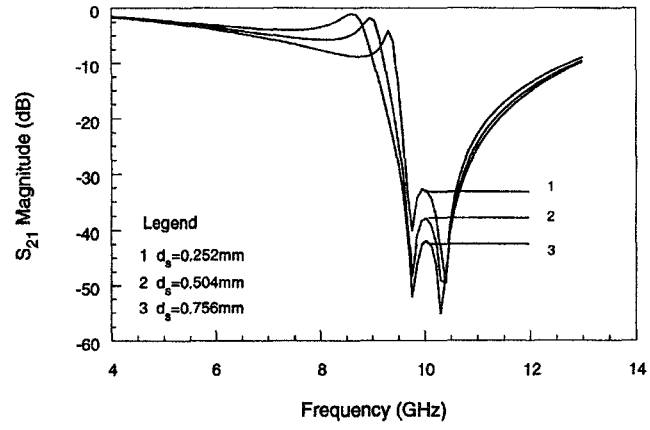

Fig. 7. Iterative double-stub notch filter design: d_s changing.

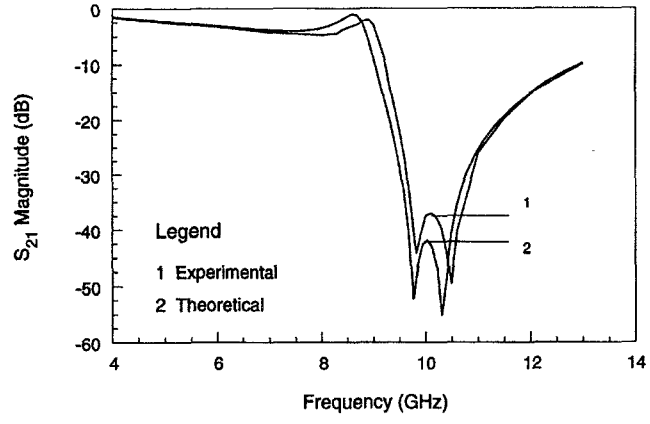

Fig. 8. Vaildation of the optimal filter design with experiment.

after the fifth iteration. Computationally, instead of solving the linear systems of order $(N + iN_d), i = 0, 1, \cdots, r$ and $N = N_i + N_o + N_{d_0}$, which involves $\mathcal{O}((N + rN_d)^4)$ operations, using ORGE we effectively solved one $(N + rN_d)$th-order system with $\mathcal{O}((N + rN_d)^3)$ operations. For the present simulation, $N_i = N_o = 16, N_{d_0} = 4, N_d = 10$ and $r = 5$. The solution of linear system of equations using ORGE requires 7.5×10^5 complex operations, compared to 2.6×10^6 required for solving the complete problem from scratch at each iteration. Fig. 6 shows that the location of the stop-band and the notch frequency are controlled by the length of the stubs.

Fig. 7 displays the insertion loss with $Y_S = 2.916$ mm, but the stub spacing varied from $d_s = 0.252$ mm to $d_s = 0.756$ mm. We infer that the Q of the stop-band is controlled by the spacing, with $d_s = 0.756$ mm yielding attenuation close to the design specifications. Therefore, it seems that the optimal filter design has $Y_S = 2.916$ mm and $d_s = 0.756$ mm. Fig. 8 corroborates the ORGE-computed response of this optimal design with the measurements reported in [12]. Other design examples can be found in [16].

V. Concluding Remarks

An order-recursive variant of Gaussian elimination has been presented for efficient solution of linear equations, arising in the interactive design of MMIC elements because of either augmenting or decrementing the baseline matrix by block

row and column vectors corresponding to reactions associated with discontinuities. The usefulness of ORGE in a CAD environment has been demonstrated by its application to the design of a microstrip double-stub filter simulated by the moment method. The geometrical layout determined by the terminal iteration yields a response that meets the design specifications and corroborates well with measured and independently simulated results reported in literature. Accuracy of the current distribution computed using ORGE has been validated with direct calculation using the well-known mixed potential integral equation approach. ORGE speeds up interactive design and circuit de-embedding by up to a factor of N/c—where N is the order of the circuit model and c is a constant considerably smaller than N. ORGE is anticipated to be very useful in the simulation, optimization, and CAD of microwave circuits.

REFERENCES

[1] J. R. Mosig, "Integral equation technique," in *Numerical Techniques for Microwave and Millimeter-Wave Passive Structures*, T. Itoh, Ed. New York: Wiley, 1989, pp. 133–213,

[2] T. K. Sarkar, Z. A. Maricevic, and M. Kahrizi, "An accurate de-embedding procedure for characterizing discontinuities," *Int. J. Microwave and Millimeter-Wave Comp. Aided Eng.*, vol. 2, no. 3, pp. 135–143, 1992.

[3] R. W. Jackson, "Full-wave finite-element analysis of irregular microstrip discontinuities," *IEEE Trans. Microwave Theory Tech.*, vol. 37, pp. 81–89, Jan. 1989.

[4] R. H. Jansen, "The spectral-domain approach for microwave integral circuits," *IEEE Trans. Microwave Theory Tech.*, vol. MTT-33, pp. 1043–1056, Oct. 1985.

[5] J. C. Rautio and R. F. Harrington, "An electromagnetic time-harmonic analysis of shielded microstrip circuits," *IEEE Trans. Microwave Theory Tech.*, vol. MTT-35, pp. 726–730, Aug. 1987.

[6] T. Becks and I. Wolff, "Analysis of 3-D metallization structures by a full-wave spectral domain technique," *IEEE Trans. Microwave Theory Tech.*, vol. 40, pp. 2219–2227, Dec. 1992.

[7] T. Itoh and R. Mittra, "Spectral-domain approach for calculating the dispersion characteristics of microstrip lines," *IEEE Trans. Microwave Theory Tech.*, vol. MTT-21, pp. 496–499, July 1973.

[8] L. P. Dunleavy and P. B. Katehi,"Shielding effects in microstrip discontinuities," *IEEE Trans. Microwave Theory Tech.*, vol. 36, pp. 1767–1774, Dec. 1988.

[9] T.-S. Horng, W. E. McKinzie, and N. G. Alexopoulos, "Full-wave spectral-domain analysis of compensation of microstrip discontinuities using triangular subdomain functions," *IEEE Trans. Microwave Theory Tech.*, vol. 40, pp. 2137–2147, Dec. 1992.

[10] F. Olyslager, D. De Zutter, and K. Blomme, "Rigorous analysis of the propagation characteristics of general lossless and lossy multiconductor transmission lines in multilayered media," *IEEE Trans. Microwave Theory Tech.*, vol. 41, pp. 79–88, Jan. 1993.

[11] K. Naishadham and T. W. Nuteson, "Efficient analysis of passive microstrip elements in MMICs," *Int. J. Microwave and Millimeter-Wave Comp. Aided Eng.*, vol. 4, no. 3, pp. 219–229, 1994.

[12] D. C. Chang and J.-X. Zheng, "Electromagnetic modeling of passive circuit elements in MMIC," *IEEE Trans. Microwave Theory Tech.*, vol. 40, pp. 1741–1747, Sept. 1992.

[13] P. Misra, "Order recursive Gaussian elimination," *IEEE Trans. Aero. Electron. Syst.*, vol. AES-32, no. 1, pp. 396–401, Jan. 1996.

[14] A. W. Glisson and D. R. Wilton, "Simple and efficient numerical methods for problems of electromagnetic radiation and scattering from surfaces," *IEEE Trans. Antennas Propagat.*, vol. AP-28, pp. 593–603, Sept. 1980.

[15] K. Naishadham and P. Misra, "Order recursive method of moments: A powerful computational tool for microwave CAD and optimization," in *IEEE Microwave Symp. Dig.*, June 1996, pp. 1463–1466.

[16] K. Naishadham and P. Misra, "Order recursive method of moments (ORMoM) for iterative design applications," *IEEE Trans. Microwave Theory Tech.*, vol. 44, pt. 2, no. 12, pp. 2595-2604, Dec. 1996.

[17] A. Skrivervik and J. R. Mosig, "Impedance matrix of multiport microstrip discontinuities including radiation effects," *AEU (Electronics and Communication)*, vol. 44, no. 6, pp. 453–461, 1990.

[18] D. M. Sheen, S. M. Ali, M. D. Abouzahra, and J. A. Kong, "Application of the three-dimensional finite-difference time-domain method to the analysis of planar microstrip circuits," *IEEE Trans. Microwave Theory Tech.*, vol. 38, pp. 849–857, July 1990.

[19] I. Park, R. Mittra, and M. I. Aksun, "Numerically efficient analysis of planar microstrip configurations using closed-form Green's functions," *IEEE Trans. Microwave Theory Tech.*, vol. 43, pp. 394–400, Feb. 1995.

[20] K. Naishadham and X. P. Lin, "Application of spectral domain Prony's method to the FDTD analysis of planar microstrip circuits," *IEEE Trans. Microwave Theory Tech.*, vol. 42, pp. 2391–2398, Dec. 1994.

[21] G. Matthaei, L. Young, and E. M. T. Jones, *Microwave Filters, Impedance-Matching Networks, and Coupling Structures*. Dedham, MA: Artech House, 1980, pp. 725–774.

[22] P. Misra, "Block recursive Gaussian elimination and LU decomposition for solution of dense systems of equations," Wright State Univ. Internal Rep. CECS/EE/1995-101, 1995.

Pradeep Misra (S'84–M'86–S'87–M'87) received the B. Tech. (Hons.) degree in electrical engineering from Indian Institute of Technology, Kharagpur, and the Ph.D. degree from Concordia University, Montréal, P.Q., Canada.

He joined Wright State University, Dayton, OH, in 1987, where he is currently an Associate Professor of Electrical Engineering. His research interests are in analysis and design of multivariable control theory, applied numerical analysis and computational techniques in controls, communications, and electromagnetics. He has published several papers in these areas and many of his algorithms have been incorporated in control design software packages.

Dr. Misra has served in various capacities in the IEEE Control Systems Society and is presently a Member of its Executive Committee.

Krishna Naishadham (S'83–M'87) received the M.S. degree from Syracuse University, Syracuse, NY, and the Ph.D. degree from the University of Mississippi, Jackson, both in electrical engineering, in 1982 and 1987, respectively.

From 1987 to 1990, he was an Assistant Professor in Electrical Engineering at the University of Kentucky, Lexington. In August 1990, he joined the Department of Electrical Engineering, Wright State University, Dayton, OH, where he is currently an Associate Professor. His research interests are in the areas of computational electromagnetics, design and analysis of microwave and millimeter-wave integrated circuits (MMIC's), prediction of EMI in printed circuit boards, and electronic materials.

Dr. Naishadham is a member of Eta Kappa Nu and Phi Kappa Phi and an elected member of URSI Commision B. He serves on the Analytical and Numerical Methods Committee (Comm. P) of the IEEE Microwave Theory and Techniques Society. He received the Best Session Paper award at the 7th SAMPE Conference on Electronic Materials.